Supporting Information

Effect of External Electric Field on Electronic Properties of $MSi_2P_xAs_y$ Monolayer and Homojunction: A First-Principal Study

Long Lai [a], Jianwei Wang [a,b,1], and Xiaobin Niu [a,2]

[a]School of Materials and Energy, University of Electronic Science and Technology of China, Chengdu 610054, P.R. China

[b]Key Laboratory of Quantum Physics and Photonic Quantum Information, the Ministry of Education, UESTC, Chengdu 611731, P. R. China

S1. Lattice constant and bandgap of $MSi_2P_xAs_y$ materials

[1] Corresponding author: jianwei_wang@uestc.edu.cn

[2] Corresponding author: xbniu@uestc.edu.cn

Table S1 the lattice constant and bandgap of $MSi_2P_xAs_y$ materials

Structure	Lattice constant(Å)	Bandgap(eV)	Lattice constant(Å)[1]	Bandgap (eV)[1]
$MoSi_2P_2As_2$	3.54	0.551	3.56	0.583
$MoSi_2P_3As$	3.52	0.534	3.54	0.576
$MoSi_2PAs_3$	3.57	0.570	3.59	0.580
$MoSi_2PAsPAs$	3.54	0.561	3.57	0.583
$MoSi_2P_2AsP$	3.50	0.629	3.52	0.648
$MoSi_2As_2PAs$	3.59	0.496	3.61	0.527
$WSi_2P_2As_2$	3.55	0.245	3.58	0.272
WSi_2P_3As	3.52	0.226	3.55	0.260
WSi_2PAs_3	3.58	0.255	3.60	0.268
$WSi_2PAsPAs$	3.55	0.247	3.58	0.272
WSi_2P_2AsP	3.50	0.325	3.53	0.331
WSi_2As_2PAs	3.58	0.196	3.62	0.231

S2. Electrostatic potential distributions across the monolayer structures

Upon completion of geometry optimization, the electrostatic potential distribution was systematically calculated for each structure. As illustrated in Figure S1, the potential distribution along the z-axis reveals a distinct asymmetry for each structure. Notably, the P_2As_2 configuration exhibits the largest electrostatic potential difference (approximately 0.25 V), while the PAsPAs configuration shows the smallest electrostatic potential variation (approximately 0.15 V). This variation suggests the presence of an intrinsic electric field within the system, which is closely linked to the atomic arrangement of the monolayer.

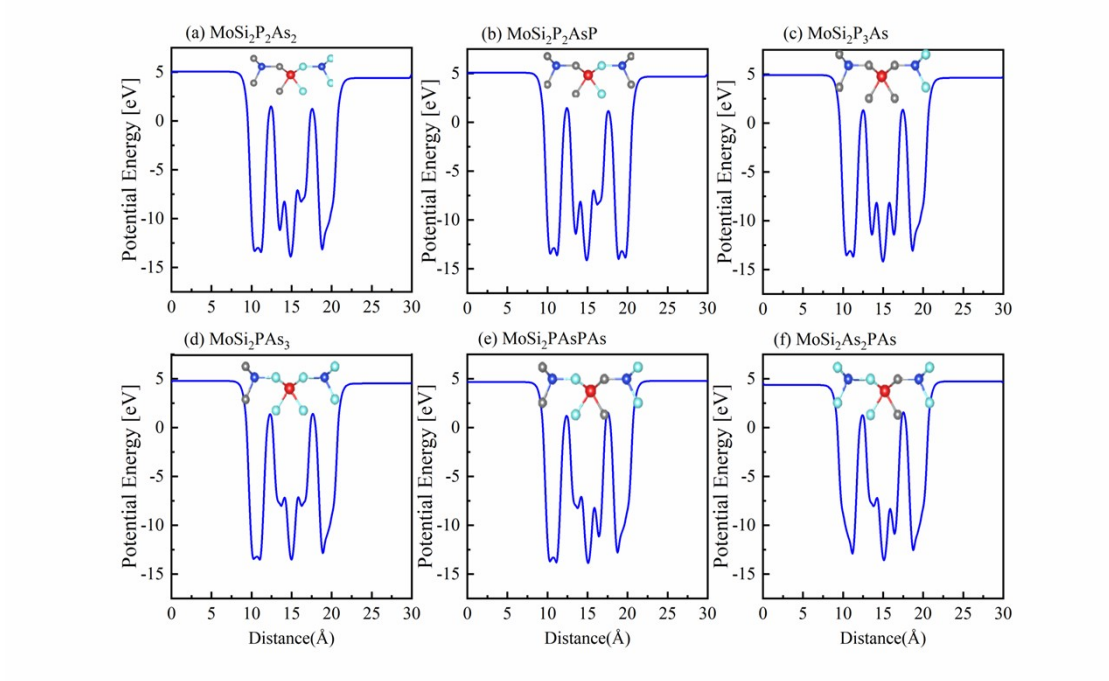

Figure S1. The electrostatic potential distribution of the six different vertical configurations of $MoSi_2P_xAs_y$ (M=Mo, W; x + y=4) materials

S3. Effect of electric field on the hybridization between Mo/W d_z^2 and As p_z components

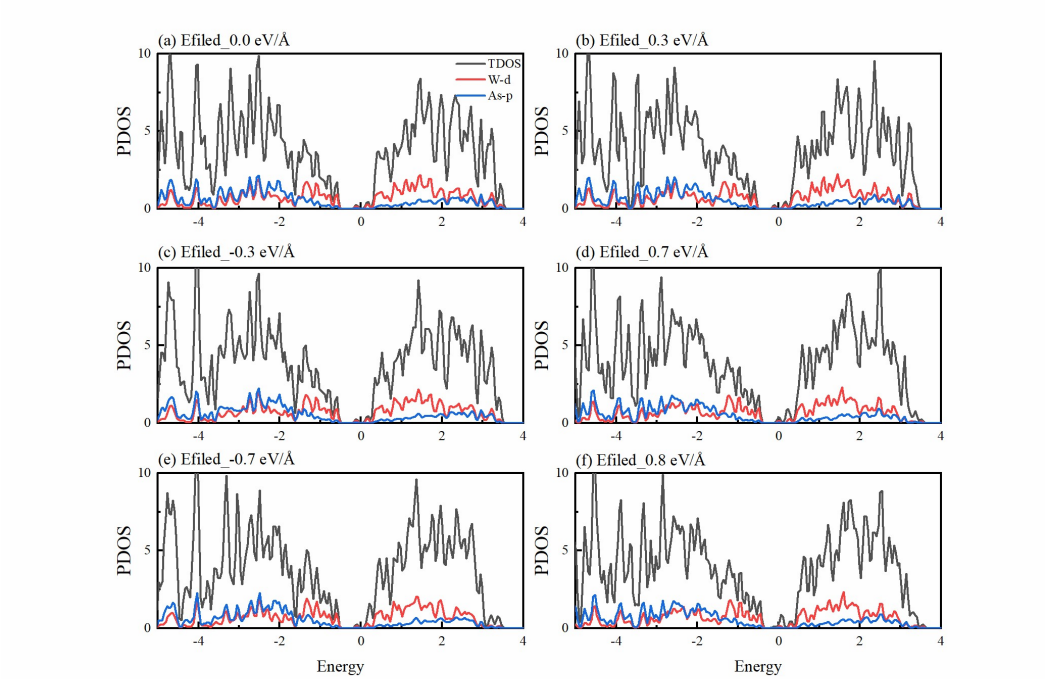

Figure S2. Projected density of states (PDOS) (a-f) of monolayer WSi_2PAs_3 as function of external electric field.

As illustrated in Figure S2, the projected density of states (PDOS) of Mo-d and As-p orbitals is analyzed under equilibrium conditions and in the presence of external electric fields ranging from 0.6 V/Å to 0.7 V/Å. In the absence of an applied field, the CBM is primarily derived from Mo-d orbitals, while the VBM arises from a hybridization between Mo-d and As-p orbitals. This hybridization indicates a strong covalent interaction between the Mo and As atoms.

S4. Derivation of k.p Hamiltonian and analysis

We use IRVSP[2] and VASP2KP[3] software to calculate the irreducible representations of CBM and VBM and construct two-band ***k.p*** model for the states around the gamma and K point.

The VASP2KP computational workflow provides an automated framework for deriving low-energy ***k.p*** models and g-factors of materials from first-principles calculations. The procedure begins with the VASP software package performing density functional theory (DFT) calculations to obtain the eigenvalues ($^{\varepsilon_n(k_0)}$) and eigenstates ($|n(k_0)\rangle$) at a specific high-symmetry ^{k_0}-point. These results are stored in the WAVECAR and EIGENVAL files, which serve as foundational data for all subsequent operations.

Subsequently, the IRVSP module conducts symmetry analysis. First, it determines the irreducible representations (irreps) of the targeted low-energy states under the little group of k_0. It then retrieves the standard matrix representations ($^{D_{std}(R)}$) of these irreps from the Bilbao Crystallographic Server (BCS). The mat2kp.in file contains this essential symmetry information.

The vasp2mat utility then processes the first-principles wavefunctions to compute the numerical matrix elements required for constructing the tight-binding Hamiltonian. The final and central component, the mat2kp module, executes the core analytical steps.

It determines a unitary transformation matrix, U, that satisfies $D_{std}(R) = U^{-1} D_{num}(R) U$ for all symmetry operations R_i in the little group.

It then constructs the effective ***k.p*** Hamiltonian (H^{kp-num}) and the Zeeman coupling term (H^{Z-num}) with numerical coefficients derived from the ab initio matrix elements.

It generates standard forms of the Hamiltonians (H^{kp-std} and H^{Z-std}) with undetermined parameters based on the symmetry constraints of the standard irreps. Finally, it solves the equation $H^{std} = U^{-1} H^{num} U$ to fit all the physical parameters (e.g., effective masses, band couplings and g-factors) of the effective model.

Table S2. The irreducible representations of the VBM

The band index	Γ	**K**
41	**Γ6**	**K4**
42	**Γ6**	**K6**

The little group of Γ point is D_{3h}.The symmetry allowed Hamiltonian considering the terms up to second order. $H_\Gamma(k)$ is given behind:

$$H_\Gamma(k) = \begin{bmatrix} H_{11} & H_{12} \\ H_{21} & H_{22} \end{bmatrix}$$

in which

$$H_{11} = a_1 + c_1(k_x^2 + k_y^2)$$

$$H_{12} = b_1((1+\sqrt{3}i)k_x + (\sqrt{3}-i)k_y)$$

$$H_{21} = b_1((1-\sqrt{3}i)k_x + (-\sqrt{3}+i)k_y)$$

$$H_{22} = a_1 + c_1(k_x^2 + k_y^2)$$

$$a_1 = -0.7432$$
$$b_1 = 0.04$$
$$c_1 = -1.7708$$

The symmetry of K point allowed Hamiltonian considering the terms up to third order.

$$H_K(k) = \begin{bmatrix} H_{11} & H_{12} \\ H_{21} & H_{22} \end{bmatrix}$$

$$H_{11}^{kp} = a_1 + a_2 + (c_1 + c_3)(k_x^2 + k_y^2) + d_1(-3k_x k_y^2 + k_x^3) + d_3(-3k_x k_y^2 + k_x^3)$$

$$H_{12}^{kp} = b_1\left(\left(1 - \frac{\sqrt{3}i}{3}\right)k_x + \left(-\frac{\sqrt{3}}{3} - i\right)k_y\right) + c_2\left(\left(\frac{2\sqrt{3}}{3} + 2i\right)k_x k_y + \left(1 - \frac{\sqrt{3}i}{3}\right)k_x^2 + \left(-1 + \frac{\sqrt{3}i}{3}\right)k_y^2\right)$$
$$+ d_2\left(\left(1 - \frac{\sqrt{3}i}{3}\right)k_x k_y^2 + \left(-\frac{\sqrt{3}}{3} - i\right)k_x^2 k_y + \left(1 - \frac{\sqrt{3}i}{3}\right)k_x^3 + \left(-\frac{\sqrt{3}}{3} - i\right)k_y^3\right)$$

$$H_{22}^{kp} = a_1 - a_2 + c_1\left(k_x^2 + k_y^2\right) + c_3\left(-k_x^2 - k_y^2\right) + d_1\left(-3k_x k_y^2 + k_x^3\right) + d_3\left(3k_x k_y^2 - k_x^3\right)$$

$a_1 = -0.1013$
$a_2 = -0.2518$
$b_1 = -0.0061$
$c_1 = -16.305$
$c_2 = -0.0742$
$c_3 = 10.5445$
$d_1 = -30.0184$
$d_2 = 1.0397$
$d_3 = 17.9875$

Symmetry analysis

Table S3: The transformations of (σ_x, σ_y, σ_z) and (k_x, k_y, k_z) with respect to the generators of the D_{3h} point group and time-reversal operator (T). Only these generators along with time-reversal operation $T = i\sigma_y K$ (K is complex conjugation operator) are considered to construct the k.p model. The last row shows the terms which are invariant under point group operation.

	$C_{3z} = e^{-i\pi/3\sigma_z}$	$M_{yz} = i\sigma_x$	$M_{xy} = i\sigma_z$	T= $i\sigma_z K$
k_x	$-k_x/2 + \sqrt{3}k_y/2$	$-k_x$	k_x	$-k_x$
k_y	$\sqrt{3}k_x/2 - k_y/2$	k_y	k_y	$-k_y$
k_z	k_z	k_z	$-k_z$	$-k_z$
σ_x	$-\sigma_x/2 + \sqrt{3}\sigma_y/2$	σ_x	$-\sigma_x$	$-\sigma_x$
σ_y	$-\sqrt{3}\sigma_x/2 - \sigma_y/2$	$-\sigma_y$	$-\sigma_y$	$-\sigma_y$
σ_z	σ_z	$-\sigma_z$	σ_z	$-\sigma_z$
E_z	E_z	E_z	$-E_z$	E_z
Invariants	$E_z(k_x\sigma_y - k_y\sigma_x)$, $E_z k_y(3k_x^2 - k_y^2)\sigma_z$, $E_z k_x(k_x^2 - 3k_y^2)\sigma_z$, $(k_x\sigma_y - k_y\sigma_x)$, $k_y(3k_x^2 - k_y^2)\sigma_z$, $k_x(k_x^2 - 3k_y^2)\sigma_z$	$k_i^m k_x\sigma_y, k_i^m k_x\sigma_z$, $k_i^m k_y\sigma_x, k_i^m k_z\sigma_x$ (i = x, y, z; m = 0, 2)	$k_i^m k_x\sigma_z, k_i^m k_y\sigma_z$, $k_i^m k_z\sigma_x, k_i^m k_z\sigma_y$ (i = x, y, z; m = 0, 2)	$k_i\sigma_j$ *(i, j=x, y, z)*

E_z linear term $E_z(k_x\sigma_y - k_y\sigma_x)$, which is Rashba spin spilting.

Table S4: The transformations of (σ_x, σ_y, σ_z) and (k_x, k_y, k_z) with respect to the generators of the C_{3h} point group.

	$C_{3z} = e^{-i\pi/3\sigma_z}$	$M_{xy} = i\sigma_z$
k_x	$-k_x/2 + \sqrt{3}k_y/2$	k_x
k_y	$-\sqrt{3}k_x/2 - k_y/2$	k_y
k_z	k_z	$-k_z$
σ_x	$-\sigma_x/2 + \sqrt{3}\sigma_y/2$	$-\sigma_x$
σ_y	$-\sqrt{3}\sigma_x/2 - \sigma_y/2$	$-\sigma_y$
σ_z	σ_z	σ_z
E_z	E_z	$-E_z$
Invariants	$E_z k_z$, $E_z(k_x\sigma_y - k_y\sigma_x)$, $(k_x\sigma_y - k_y\sigma_x)$,	$k_i^m k_x\sigma_z, k_i^m k_y\sigma_z$, $k_i^m k_z\sigma_x, k_i^m k_z\sigma_y$

$k_y\left(2k_x^2 - k_y^2\right)\sigma_z, k_x\left(k_x^2 - 3k_y^2\right)\sigma_z$	(i = x, y, z; m = 0, 2)

S5. Electrostatic potential profiles for homojunctions.

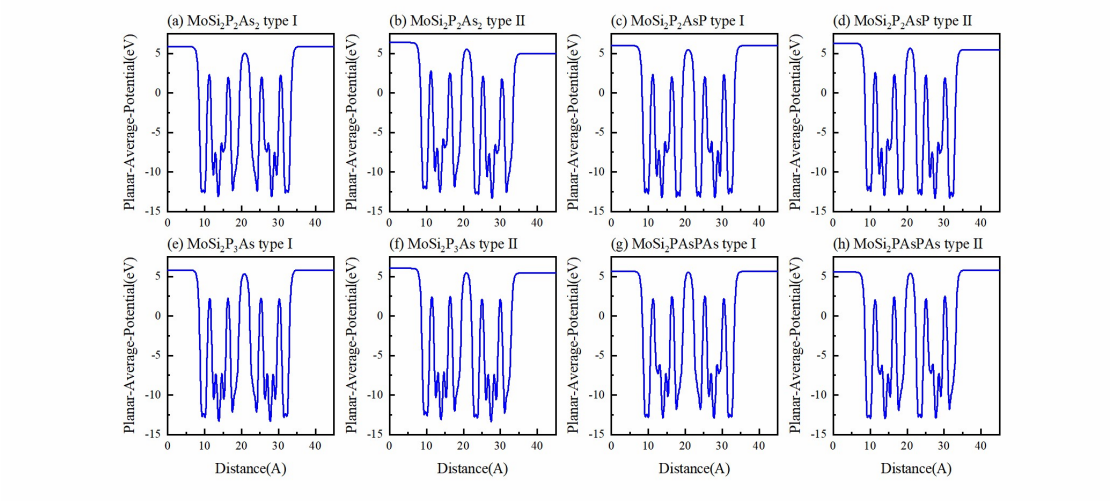

Figure S3. The part of the electrostatic potential of the homojunction

Reference

1. A. Rezavand, N. Ghobadi and B. Behnamghader, Electronic and spintronic properties of Janus $MSi_2P_xAs_y$ (M = Mo, W) monolayers, *Phys. Rev. B*, 2022, **106**, 035417.
2. J. Gao, Q. Wu, C. Persson and Z. Wang, Irvsp: To obtain irreducible representations of electronic states in the VASP, *Comput. Phys. Commun.*, 2021, **261**, 107760.
3. S. Zhang, H. Sheng, Z.-D. Song, C. Liang, Y. Jiang, S. Sun, Q. Wu, H. Weng, Z. Fang, X. Dai and Z. Wang, VASP2KP: k·p Models and Landé g-Factors from ab initio Calculations, *Chin. Phys. Lett.*, 2023, **40**, 127101.